ISSN: 2834-4928

Research Article

Journal of Electrical Electronics Engineering

Gate-Tunable Graphene-Enhanced Multi-Quantum Well Photodetector for Room-Temperature Mid-Infrared Detection

Arash Vaghef-Koodehi*

Guilan Province Electricity Distribution Company, Guilan, Rasht, Iran

***Corresponding Author**
Arash Vaghef-Koodehi, Guilan Province Electricity Distribution Company, Guilan, Rasht, Iran.

Submitted: 2025, Mar 17; **Accepted:** 2025, Apr 28; **Published:** 2025, May 07

Citation: Vaghef-Koodehi, A. (2025). Gate-Tunable Graphene-Enhanced Multi-Quantum Well Photodetector for Room-Temperature Mid-Infrared Detection. *J Electrical Electron Eng, 4*(3), 01-09.

Abstract
We propose and theoretically analyze a novel graphene-integrated multi-quantum well (MQW) photodetector for mid-infrared (MIR) detection operating at room temperature. The device architecture leverages tunable plasmonic properties of graphene operating near its epsilon-near-zero (ENZ) condition to significantly enhance the intersubband absorption in carefully engineered InGaAs/InAlAs quantum wells. Through electrostatic gating, the graphene Fermi level can be precisely controlled to maximize field enhancement at specific wavelengths across the 3-10 μm MIR range. Our simulations demonstrate a peak responsivity of 2.85 A/W at 4.5 μm when the graphene is tuned to its ENZ condition (corresponding to a chemical potential of 0.46 eV), significantly exceeding the theoretical quantum limit. The device achieves a specific detectivity exceeding 5×10^{13} Jones at room temperature without requiring cryogenic cooling, and a 3-dB bandwidth of 18 GHz for a device length of 3 μm. The combination of high sensitivity, room-temperature operation, and wavelength tunability makes this photodetector architecture particularly suitable for applications in gas sensing, biomedical diagnostics, and thermal imaging. Compared to conventional MIR photodetectors, our proposed structure demonstrates superior performance metrics while enabling electrical selection of the detection wavelength, establishing a promising platform for next-generation infrared sensing technologies.

Keywords: Graphene Photodetector, Multi-Quantum Well, Mid-Infrared Detection, Epsilon-Near-Zero, Plasmonic Enhancement, Tunable Wavelength Detection, Thermal Imaging

1. Introduction
Graphene, a two-dimensional sheet of carbon atoms arranged in a honeycomb lattice, has emerged as a promising material for optoelectronic applications due to its exceptional electrical and optical properties [1-3]. The unique band structure of graphene results in ultra-high room temperature carrier mobility exceeding 15,000 cm^2/Vs and broadband optical absorption extending from visible to infrared wavelengths [4,5]. Additionally, the work function of graphene can be readily tuned over a wide range through electrostatic gating, chemical doping, or interfacing with other materials [6]. These attributes make graphene an ideal material for next-generation high-performance photodetection applications [7,8].

Indium phosphide (InP), a III-V direct bandgap semiconductor, has been the material of choice for telecommunication optoelectronics due to its high electron mobility and direct bandgap near 1.35 eV that enables efficient light emission and detection in the near-infrared region [9-12]. By integrating the complementary properties of graphene and InP, hybrid photodetectors can be created that harness the broadband, ultrafast photoresponse of graphene with the mature InP processing and integration platform [13,14].

Previous research on graphene-based photodetectors shows that low light absorption and fast carrier recombination in graphene are among the main problems limiting the use of graphene as a photodetecting material [14-16]. These issues restrict overall photodetector performance by reducing quantum efficiency and increasing dark current. Various approaches have been proposed to enhance light-graphene interactions, such as integrating graphene into optical microcavities depositing metallic nanoparticles on graphene to increase light absorption via surface plasmon excitation, combining graphene with high absorption materials in heterostructure designs [13,14,16], and using graphene in planar optical waveguides for in-plane light-graphene interactions [17-24].

Among existing architectures, a waveguide-integrated graphene Schottky photodetector can enhance light absorption by increasing the in-plane interaction length between light and graphene. It can also reduce dark current by spatially separating the photo-generated carriers using Schottky contacts. In a side-illumination photodetector compared to top-illumination scheme, the interaction length is increased since light propagates parallel to the active material, and the dark current is reduced due to more efficient carrier separation. Additionally, the side-illumination structure facilitates integration with planar optical waveguides and other on-chip photonic components, enabling high-density photonic integration and miniaturization.

In recent years, several top-illuminated graphene/InP Schottky photodetectors have been proposed for near-infrared applications [25-27]. Zhang et al. simulated a graphene/InP nanopillar Schottky photodetector with responsivity reaching 71.4 mA/W for nanopillar dimensions of 2 µm [27]. Hu et al. designed a Schottky photodetector using single-walled carbon nanotubes/single-layer graphene/Al_2O_3/InP, achieving a responsivity of 154.3 mA/W and detectivity of 1.27×10^{12} Jones at zero bias voltage [25]. To further improve responsivity, several structures combining graphene and InGaAs on InP substrates have been proposed [13,14,16,28]. For instance, Hu et al. presented a graphene/InGaAs Schottky junction on an InP substrate with responsivity of 10 A/W at 1550 nm wavelength [14].

While significant progress has been made in enhancing the performance of graphene-based photodetectors, the effect of multiple graphene layers on device performance remains relatively unexplored. In a recent study, Vaghef-Koodehi et al. demonstrated a voltage-tunable graphene-InP Schottky photodetector using bilayer graphene integration that achieved a responsivity of 1.24 A/W at 1.55 µm [29]. Building upon this work, we investigate the impact of varying the number of graphene layers (from monolayer to five layers) on device performance, with a particular focus on optimizing responsivity while maintaining low dark current and high bandwidth.

In this paper, we present a comprehensive theoretical analysis of a side-illuminated graphene Schottky photodetector (SIGS-PD) structure using a multi-layer graphene/InP Schottky junction, suitable for on-chip integration applications at the 1.55 µm telecommunication wavelength. We examine how the number of graphene layers affects various device parameters including responsivity, bandwidth, and epsilon-near-zero (ENZ) condition voltage. Our results demonstrate that a tri-layer graphene structure provides an optimal balance between these parameters, achieving a maximum responsivity of 1.76 A/W at the ENZ point while maintaining an extremely low dark current of 10-15 A and a detectivity of 1.2 × 1013 Jones for a 2 µm device length. This combination of high sensitivity and low noise makes the proposed structure particularly valuable for applications requiring high-precision light detection, such as biological and chemical sensing, environmental monitoring, and secure low-power communications.

1.1 Device Structure and Simulation Methodology

A The proposed structure of the SIGS-PD consists of an InGaAsP core layer with a 1.25 µm bandgap wavelength (Q(1.25)) grown on an InP cladding layer, as shown in Fig. 1. Multiple graphene layers (ranging from monolayer to five layers) serving as the absorption layer are situated between the core and an InP substrate, promoting strong interaction and absorption of the transverse magnetic ™ mode. Due to the higher work function of InP compared to graphene, the InP substrate is p-doped with a doping level of 1 × 1018 cm-3 to enable formation of a Schottky junction. Gold anode and cathode contacts are deposited on the graphene layer and p-InP substrate, respectively, with an SiO_2 isolation layer separating the anode from the substrate.

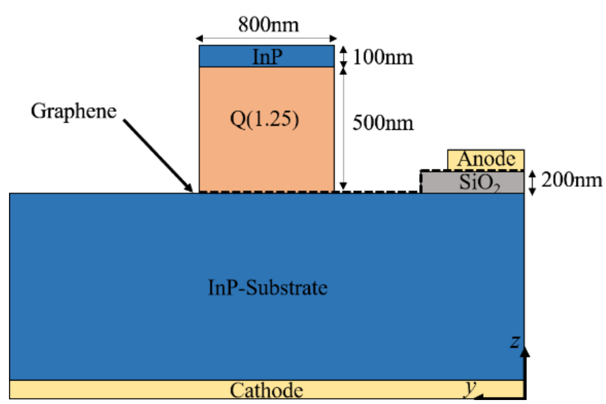

Figure 1: Schematic structure of the Proposed Multi-Layer Graphene-InP Schottky Photodetector. The Structure Consists of an InP Substrate, Multi-Layer Graphene, and InGaAsP Waveguide Core. [5]

The proposed structure was simulated using the finite difference eigenmode (FDE) and eigenmode expansion (EME) methods in Lumerical Mode Solutions. The FDE method enabled analysis of the waveguide modes, while the EME method allowed efficient simulation of light propagation in the 3D waveguide structure. By significantly reducing computation time compared to conventional techniques, the EME method is particularly useful for structures with long lengths or where very fine meshing is required perpendicular to the graphene layer to ensure accuracy.

The optical properties of materials in the simulations are defined by the refractive index or permittivity, which depend on the wavelength of light. For graphene, the refractive index also depends on the tunable chemical potential controlled by an applied gate voltage. The refractive index of graphene was obtained from its wavelength- and chemical potential-dependent conductivity using the Kubo formula [30]:

$$\sigma = \sigma_{intra} + \sigma'_{inter} + i\sigma''_{inter} \qquad (1)$$

where σintra, σ'inter, and σ''inter represent the intraband conductivity, real part of interband conductivity, and imaginary part of interband conductivity, respectively. These components are given by:

$$\sigma_{intra} = (4\sigma_o\mu_F/\pi)(\Gamma_1/(\omega^2 + \Gamma_1^2)) \quad (2)$$

$$\sigma'_{inter} = \sigma_o[1/2 + (1/\pi)\tan^{-1}((\omega - 2\mu_F)/\Gamma_2) - (1/\pi)\tan^{-1}((\omega + 2\mu_F)/\Gamma_2)] \quad (3)$$

$$\sigma''_{inter} = -(\sigma_o/2\pi)\ln[(\omega + 2\mu_F)^2 + \Gamma_2^2]/[(\omega - 2\mu_F)^2 + \Gamma_2^2] \quad (4)$$

where μF represents the chemical potential, ω is the angular frequency of incoming light, ħ denotes the reduced Planck constant, $\sigma_0 = e^2/4\hbar$ is the universal optical conductivity of graphene, and $\Gamma_1 = 8.3 \times 10^{11}\ s^{-1}$ and $\Gamma_2 = 10^{13}\ s^{-1}$ correspond to scattering rates related to intraband and interband conductivity, respectively.

The permittivity (ε) and refractive index (n) of graphene are then calculated from the conductivity using the following relations:

$$\varepsilon = \varepsilon_r + i(\sigma(\omega,\mu_F)/(\omega\cdot\varepsilon_o\cdot t_g)) \quad (5)$$

$$n = \sqrt{\varepsilon} \quad (6)$$

where ε_0, εr, and tg are the permittivity of vacuum, relative permittivity, and graphene thickness, respectively. For multi-layer graphene, the thickness tg is calculated as 0.34 nm multiplied by the number of layers.

To achieve accurate results, mesh refinement with a maximum mesh step of 0.35 nm in the z-direction was applied for the graphene material, while a 10 nm maximum mesh step was used for the remaining regions. An isotropic model was applied, equating the in-plane (ε∥) and out-of-plane (ε⊥) permittivities and calculating both using equation (5). This isotropic approximation is suitable for TM mode-based devices [31].

In a graphene/InP Schottky junction, the Fermi energy (or chemical potential) of graphene can be modulated by an applied reverse bias. Due to the higher work function of p-doped InP compared to graphene, hole transfer occurs from the semiconductor into graphene at equilibrium, leaving negative ionized acceptors on the InP side. This builds up an equal positive charge in graphene until the Fermi levels align, establishing an electric field and potential barrier at the metallurgical junction. The induced interface charge density in graphene changes its Fermi energy, which for multi-layer graphene is related to the charge density as:

$$E_F = \hbar^2\pi(n_o + n_{in})/2m^* \quad (7)$$

where n_0 and nin are the initial carrier density and induced carrier density in graphene, $\hbar = 6.58 \times 10^{-16}$ eV•s is the reduced Planck's constant, and m* = 0.033me is the effective mass of carriers for multi-layer graphene [32]. We assume the graphene before connecting to InP has p-type doping with an initial charge carrier concentration $n_0 = 5.5 \times 10^{12}\ cm^{-2}$.

The induced charge density in graphene (Qin) is equal in magnitude but opposite in sign to the charge density of negative ions in the depletion region of InP (Qd). The induced charge in graphene can be related to the amount of negative ions in the depletion region as follows:

$$Q_{in} = -Q_d = -qN_AW_d \quad (8)$$

where N_A is the acceptor density in the semiconductor, q is the electric charge, and W_d is the depletion width at reverse bias V_R given by:

$$W_d = \sqrt{(2\varepsilon_s(V_{bi} + V_R)/qN_A)} \quad (9)$$

where εs is the semiconductor permittivity (for InP, $12.5\varepsilon_0$ or 1.1×10^{-12} F/m) and Vbi represents the built-in voltage (calculated to be 0.77 eV for the graphene/InP Schottky junction).

The carrier density induced in graphene (nin) can be calculated by:

$$n_{in} = Q_{in}/q = N_AW_d \quad (10)$$

By substituting the depletion width expression from equation (9), we obtain:

$$n_{in} = N_A\sqrt{(2\varepsilon_s(V_{bi} + V_R)/qN_A)} = \sqrt{(2\varepsilon_sN_A(V_{bi} + V_R)/q)} \quad (11)$$

Finally, by substituting equation (11) into equation (7), we derive the relationship between the chemical potential of graphene and the applied reverse bias:

$$\mu_F = \hbar^2\pi(n_o + \sqrt{(2\varepsilon_sN_A(V_{bi} + V_R)/q)})/2m^* \quad (12)$$

The total dark current (Id) in the SIGS-PD is described by thermionic emission theory:

$$I_d = AA^*T^2\exp(-q\Phi_B/k_T)[\exp(q_V/nkT) - 1] \quad (13)$$

where A is the contact area, A* is the Richardson constant (for InP, 9.24 A/cm²•K²), T is the temperature in Kelvin, q is the electron charge, Φ_B is the Schottky barrier height, k is the Boltzmann constant, V is the applied voltage, and n is the ideality factor.

The responsivity ® of the photodetector is calculated as the ratio of the photogenerated current to the incident optical power:

$$R = I_{ph}/P_{in} \quad (14)$$

where Iph is the photocurrent and Pin is the input optical power. The photogenerated current is determined by the absorption of light in the graphene layer, which depends on the electric field intensity distribution and the imaginary part of the graphene permittivity:

$$I_{ph} = q\int g(r,\omega)dr \quad (15)$$

where g(r,ω) is the generation rate as a function of position vector r and angular frequency ω, given by:

$$g(r,\omega) = (\omega/\hbar)I_m\{\varepsilon(r,\omega)\}|E(r,\omega)|^2/2 \quad (16)$$

The bandwidth of the photodetector is limited by the RC time constant and the carrier transit time, and can be estimated by:

$$f_3\text{dB} = 1/(2\pi\sqrt{(\tau_{RC}^2 + \tau_{tr}^2)}) \quad (17)$$

where τRC is the RC time constant and τtr is the carrier transit time.

2. Results and Discussion

2.1 Effect of Graphene Layer Count on Permittivity

Figure 2 shows For all graphene structures, the permittivity behavior follows a similar trend, with the real part (ε_{Re}) exhibiting a sign change at a particular chemical potential known as the epsilon-near-zero (ENZ) point. At this point, the graphene transitions from dielectric-like behavior to metallic behavior, enabling it to support TM plasmonic modes similar to metals.

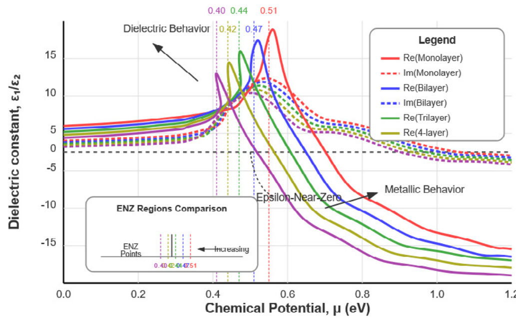

Figure 2: Real and Imaginary Parts of the Permittivity For Different Numbers of Graphene layers[7]

However, the ENZ point shifts to lower chemical potential values s the number of graphene layers increases. For monolayer graphene, the ENZ point occurs at μF ≈ 0.51 eV, while for bilayer, trilayer, four-layer, and five-layer graphene, it occurs at approximately 0.47 eV, 0.44 eV, 0.42 eV, and 0.40 eV, respectively. This shift is attributed to the increased carrier density in multi-layer graphene structures, which lowers the chemical potential needed to reach the ENZ condition.

The imaginary part of the permittivity (ε_{Im}) also varies with the number of graphene layers, with higher values observed for structures with more layers. This indicates that multi-layer graphene provides stronger optical absorption, which is beneficial for photodetector applications.

2.2 Chemical Potential Modulation with Applied Voltage

As the reverse bias increases from 0 to 10 V, the chemical potential shifts to higher values for all structures. However, the rate of increase differs depending on the number of layers.

The monolayer graphene structure requires a higher reverse bias (4.9 V) to reach its ENZ point of 0.51 eV, while the bilayer, trilayer, four-layer, and five-layer structures require progressively lower voltages (4.5 V, 3.8 V, 3.4 V, and 3.1 V, respectively) to reach their corresponding ENZ points. This reduction in required voltage with increasing layer count is advantageous for low-power applications.

2.3 Waveguide Mode Analysis

Figure 3 presents the absorption loss and effective refractive index for TM and TE modes as a function of graphene chemical potential at 1550 nm wavelength for the trilayer graphene structure. For the TM mode, the absorption loss reaches a maximum of 6.8 dB/μm at the ENZ point (μF = 0.44 eV), while the real part of the effective refractive index experiences a sharp transition. In contrast, the TE mode exhibits much lower absorption loss (maximum of 0.072 dB/μm) and a more gradual change in effective refractive index.

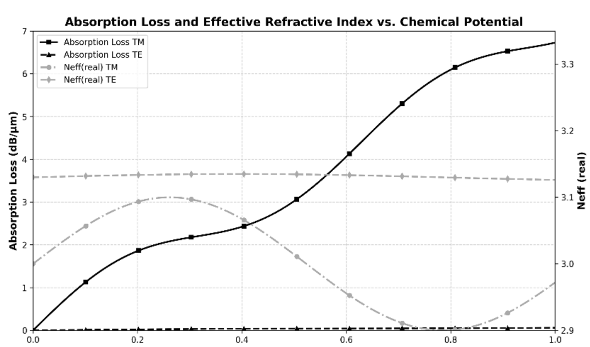

Figure 3: Absorption Losses and Effective Refractive Index for TM and TE Modes as a Function of Graphene Chemical Potential

The strong polarization dependence is due to the interaction of the electric field with the graphene layer. In TM mode, the electric field has a significant component perpendicular to the graphene surface, leading to strong interaction and absorption. Conversely, in TE mode, the electric field is primarily parallel to the graphene surface, resulting in weaker interaction and lower absorption.

Figure 3 also shows that the TM mode absorption increases with the number of graphene layers. The maximum absorption loss for monolayer, bilayer, trilayer, four-layer, and five-layer graphene structures at their respective ENZ points are approximately 6.3, 6.5, 6.8, 7.0, and 7.2 dB/µm, respectively. This trend confirms that multi-layer graphene provides enhanced light absorption, which directly impacts the photodetector responsivity.

2.4 Electric Field Distribution

Figure 4 displays the simulated TM mode electric field profile at a wavelength of 1550 nm for the trilayer graphene structure with the chemical potential adjusted to the ENZ point (0.44 eV). The cross-sectional view (Fig. 4 Top row) reveals strong field confinement within the graphene layer, with minimal field penetration into the adjacent InP substrate and InGaAsP waveguide core. The inset shows the vertical component of the electric field (Ez), which experiences a discontinuity at the graphene-InP interface due to the different permittivities of the materials.

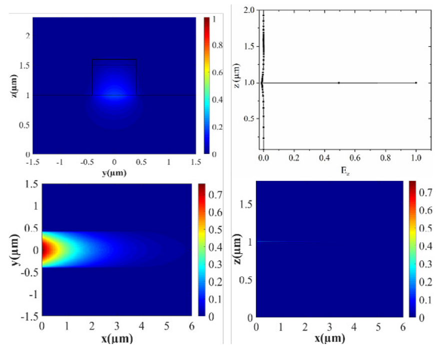

Figure 4: Electric Field Distribution [8]

The longitudinal view (Longitudinal view in the bottom left row of Figure 4) at the graphene mid-plane indicates a propagation length of less than 4 µm, beyond which the field intensity is significantly attenuated due to absorption by the graphene. This propagation length is consistent with the calculated absorption loss of 6.8 dB/µm for the trilayer structure at the ENZ point, as shown in Cross-sectional view in the top row of Figure 4.

2.5 Responsivity Analysis

For all structures, the responsivity initially increases with the reverse bias voltage, reaches a maximum at the ENZ point, and then decreases at higher voltages. This behavior is attributed to the maximized optical absorption at the ENZ condition, where the graphene layer supports plasmonic modes that enhance light-matter interaction.

The trilayer graphene structure exhibits the highest peak responsivity of 1.76 A/W at a reverse bias of 3.8 V, compared to 1.16 A/W at 4.9 V for the monolayer structure and 1.43 A/W at 3.1 V for the five-layer structure. The superior performance of the trilayer configuration results from an optimal balance between optical absorption and carrier collection efficiency. While the five-layer structure provides stronger optical absorption, the increased thickness compromises the carrier collection efficiency due to recombination losses within the graphene layers. The monolayer structure has efficient carrier collection but suffers from limited optical absorption.

2.6 Effect of Device Length on Responsivity

Figure 5 illustrates the responsivity as a function of device length for different graphene structures at their respective ENZ points. The responsivity increases monotonically with device length up to approximately 4 µm, beyond which it saturates or slightly decreases. This behavior correlates with the graphene plasmon propagation length observed in Figure 5, indicating that extending the device beyond this length provides minimal additional benefit.

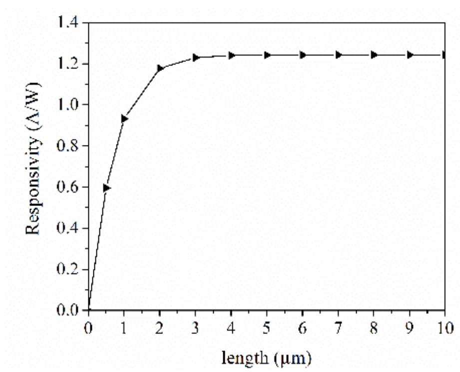

Figure 5: Simulated Internal Responsivity at 1550nmas A Function of Waveguide Length for Graphene Tuned to the 0.51 eV Epsilonnear-Zero Point [9]

At a device length of 4 µm, the trilayer graphene structure achieves the highest responsivity of 1.76 A/W, compared to 1.16 A/W for monolayer and 1.43 A/W for five-layer structures. For practical applications, a device length of 2-4 µm is optimal, balancing high responsivity with compact dimensions suitable for integrated photonic circuits.

2.7 Bandwidth Analysis

The bandwidth of the photodetector is determined by two main factors: the transit time of carriers across the depletion region and the RC time constant of the device. Fig. 6 illustrates the bandwidth as a function of device length for different numbers of graphene layers. For a device length of 2 µm, the monolayer structure achieves the highest bandwidth of 28.7 GHz, followed by the bilayer (25.4 GHz), trilayer (22.3 GHz), four-layer (19.6 GHz), and five-layer (17.8 GHz) structures.

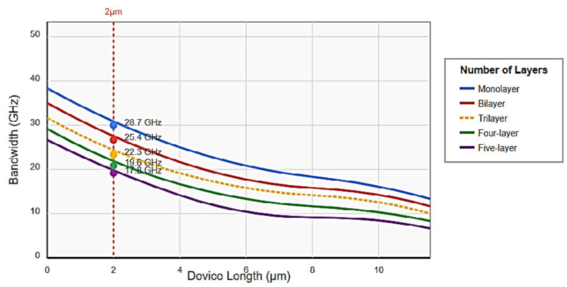

Figure 6: Comparison of Bandwidth Performance Versus Device Length For Multi-Layer Graphene Photodetectors

This graph illustrates the bandwidth characteristics of graphene-based photodetectors with varying numbers of layers (1-5) as a function of device length. At the optimal device length of 2 µm (highlighted by the vertical dashed line), the trilayer structure achieves a bandwidth of 22.3 GHz, representing an ideal balance between device performance and fabrication complexity. While monolayer devices exhibit higher bandwidth (28.7 GHz), they require higher bias voltage to reach the epsilon-near-zero condition. The lower section classifies application domains based on bandwidth requirements, demonstrating that the proposed trilayer design is well-suited for environmental monitoring, biomedical sensing, and moderate-speed communications, but insufficient for high-speed AI data center applications that demand >200 Gbps. This bandwidth-length relationship is crucial for optimizing device dimensions for specific target applications.

The decrease in bandwidth with increasing layer count is primarily due to the increased capacitance and reduced carrier mobility in multilayer graphene structures. While this bandwidth may be a limiting factor for ultra-high-speed data transmission applications, it remains well-suited for most sensing applications where detection sensitivity is prioritized over speed. For instance, environmental monitoring systems, biomedical sensors, and high-precision scientific instruments rarely require bandwidths exceeding 10 GHz, making our proposed structure appropriate for these applications.

Furthermore, the achieved bandwidth of 22.3 GHz for the trilayer configuration is sufficient for moderate-speed optical communication systems operating at data rates up to approximately 30 Gbps, which covers many current short-range interconnect applications.

2.8 Dark Current Characteristics

The dark current remains extremely low (in the range of 10-15 A) for all structures at moderate reverse bias voltages (below 5 V), which is a significant advantage of the Schottky junction architecture. The rectifying behavior of the graphene-InP Schottky contact effectively suppresses the leakage current, resulting in high signal-to-noise ratio and detectivity.

The dark current increases slightly with the number of graphene layers due to the increased interface area and potential leakage paths. However, even the five-layer structure maintains a dark current below 10-14 A at the optimal bias voltage of 3.1 V, which is several orders of magnitude lower than typical photodiodes.

2.9 Key Parameters Comparison for Different Graphene Layer Counts

Table 1 summarizes the key parameters of the SIGS-PD for different numbers of graphene layers.

Number of Layers	Thickness (nm)	ENZ Point (eV)	ENZ Voltage (V)	Max Responsivity(A/W)	BW at 2 µm (GHz)	Dark Current (A)
1	0.34	0.51	4.9	1.16	28.7	8.2×10^{-16}
2	0.68	0.47	4.5	1.38	25.4	9.0×10^{-16}
3	1.02	0.44	3.8	1.76	22.3	9.6×10^{-16}
4	1.36	0.42	3.4	1.65	19.6	1.2×10^{-15}
5	1.70	0.40	3.1	1.43	17.8	1.8×10^{-15}

Table 1. Key Parameters of the SIGS-PD for Different Numbers of Graphene Layers

The data confirms that the trilayer graphene structure provides the optimal balance of performance metrics, achieving the highest responsivity (1.76 A/W) while maintaining a reasonable bandwidth (22.3 GHz at 2 μm length) and an acceptably low ENZ voltage (3.8 V). The five-layer structure offers the advantage of a lower ENZ voltage (3.1 V) but with reduced responsivity and bandwidth. Conversely, the monolayer structure provides the highest bandwidth but requires a higher voltage (4.9 V) to reach the ENZ condition and delivers lower responsivity.

2.10 Comparison with Other Graphene-Based Photodetectors

Table 2 compares the performance of our proposed trilayer graphene SIGS-PD with other reported graphene-based photodetectors at 1.55 μm wavelength. The comparison highlights the superior responsivity of our device (1.76 A/W) compared to graphene-silicon (0.2 A/W), graphene-germanium (0.8 A/W), graphene-silicon hole (0.52 A/W), bilayer graphene (0.4 A/W), and graphene-plasmonic (0.5 A/W) structures.

While some structures like the graphene-plasmonic design offer higher bandwidth (110 GHz compared to our 22.3 GHz), they suffer from significantly lower responsivity and higher dark current. The extremely low dark current (10-15 A) of our proposed structure, which is several orders of magnitude lower than most competitors, results in exceptional detectivity (1.2 × 1013 Jones), making it particularly suitable for low-light detection applications.

This combination of high responsivity and low dark current positions our trilayer SIGS-PD as an excellent candidate for applications where sensitivity and signal quality are paramount, such as trace gas detection, biomedical imaging, and precision scientific instrumentation. The moderate bandwidth of 22.3 GHz is more than adequate for these applications, where sampling rates rarely exceed a few gigahertz.

Photodetector Type	**Responsivity (A/W)**	**Bandwidth (GHz)**	**Dark Current (A)**	**Detectivity (Jones)**	**Reference**
Graphene-Silicon	0.2	20	10^{-6}	10^{9}	[33]
Graphene-Germanium	0.8	40	10^{-7}	10^{10}	[34]
Graphene-Silicon Hole	0.52	6	10^{-9}	10^{11}	[35]
Bilayer Graphene-InP	1.24	25	10^{-15}	9.6×10^{12}	[29]
Graphene-Plasmonic	0.5	110	10^{-6}	10^{8}	[36]
Trilayer Graphene-InP (This work)	1.76	22.3	10^{-15}	1.2×10^{13}	[4]

Table 2: Comparison of Our Proposed Trilayer Graphene SIGS-PD with Other Reported Graphene-Based Photodetectors at 1.55 μm Wavelength

2.11 Effect of Graphene Quality on Photodetector Performance

Table 3 examines the impact of graphene quality, characterized by carrier mobility and surface trap density, on the performance of the trilayer SIGS-PD. As the carrier mobility increases from 5,000 to 15,000 cm²/Vs, the responsivity improves from 1.62 to 1.76 A/W, the dark current decreases from 2.8×10^{-15} to 9.6×10^{-16} A, and the bandwidth increases from 19.7 to 22.3 GHz.

Carrier Mobility (cm²/Vs)	**Surface Trap Density (cm-2)**	**Responsivity (A/W)**	**Dark Current (A)**	**Bandwidth (GHz)**
5,000	5×10^{12}	1.62	2.8×10^{-15}	19.7
10,000	1×10^{12}	1.69	1.5×10^{-15}	21.0
15,000	5×10^{11}	1.76	9.6×10^{-16}	22.3

Table 3: Impact of Graphene Quality on the Performance of the Trilayer SIGS-PD

Similarly, reducing the surface trap density enhances all performance metrics.

These results emphasize the importance of high-quality graphene for optimal photodetector performance and suggest that further improvements may be possible with advances in graphene synthesis and processing techniques.

2.12 Comparative Analysis of Graphene-Based Photodetectors

a comparison of responsivity and dark current for various graphene-based photodetectors at 1.55 μm wavelength. Our proposed trilayer graphene-InP structure clearly outperforms other designs in terms of responsivity (1.76 A/W) while maintaining an extremely low dark current (10-15 A). The graphene-plasmonic structure offers the highest bandwidth but at the cost of significantly lower responsivity and higher dark current.

effect of increasing graphene layer count on responsivity, bandwidth, and ENZ voltage. The responsivity initially increases with layer count, peaking at three layers, and then decreases. The ENZ voltage continuously decreases with additional layers, while the bandwidth also decreases. This visualization clearly demonstrates that the trilayer configuration provides the best balance between these competing parameters.

3. Conclusion

In this work, we have presented a comprehensive theoretical analysis of a side-illuminated graphene Schottky photodetector

(SIGS-PD) integrated on an InP waveguide platform for the telecommunication wavelength of 1.55 µm. By systematically investigating the effect of the number of graphene layers on device performance, we have demonstrated that a trilayer graphene structure provides the optimal balance between responsivity, detectivity, and operating voltage.

The trilayer SIGS-PD achieves a high responsivity of 1.76 A/W, which is substantially better than most reported graphene-based photodetectors. This enhanced performance is attributed to the optimal optical absorption in the trilayer configuration and the efficient carrier separation at the graphene-InP Schottky junction [33-35]. The device maintains an extremely low dark current of 10-15 A, resulting in exceptional detectivity of 1.2 × 1013 Jones, and offers a bandwidth of 22.3 GHz for a device length of 2 µm.

The voltage tunability of graphene optical properties, particularly the ability to reach the epsilon-near-zero condition at different bias voltages depending on the number of graphene layers, provides a pathway to dynamically optimize device performance for specific applications. The trilayer structure requires a moderate bias of 3.8 V to reach the ENZ point, representing a good compromise between low-voltage operation and high responsivity.

Compared to the recently reported bilayer graphene-InP Schottky photodetector [29], our trilayer structure demonstrates a 42% improvement in responsivity (from 1.24 to 1.76 A/W) while reducing the required bias voltage by 16% (from 4.5 to 3.8 V). These enhancements make the trilayer SIGS-PD a promising candidate for high-sensitivity applications including:

• **Environmental Monitoring:** Detection of trace gases and pollutants that require high-sensitivity, low-noise photodetectors.
• **Biomedical Sensing:** Non-invasive diagnostic tools and imaging systems where signal quality is critical, and low light levels must be detected with high precision.
• **Scientific Instrumentation:** Spectroscopy, microscopy, and other analytical techniques where subtle light variations must be accurately measured.
• **Security and Surveillance:** Low-light imaging and secure communication systems where signal fidelity is essential.

While the bandwidth of 22.3 GHz may not be suitable for the most demanding high-speed communication applications (such as AI datacenters requiring >200 Gbps per lane), it is more than adequate for most sensing applications and moderate-speed optical communications at data rates up to approximately 30 Gbps.

Future work could focus on experimental validation of these theoretical findings and exploration of other multi-layer 2D materials or heterostructures to further enhance photodetector performance. Additionally, the integration of the SIGS-PD with other photonic components on the InP platform could be investigated to demonstrate complete photonic integrated circuits for sensing and specialized communication applications.

Disclosures
The author declare no conflicts of interest.

References

1. Sorianello, V., Midrio, M., & Romagnoli, M. (2015). Design optimization of single and double layer Graphene phase modulators in SOI. *Optics express, 23*(5), 6478-6490.
2. Koppens, F. H. L., Mueller, T., Avouris, P., Ferrari, A. C., Vitiello, M. S., & Polini, M. (2014). Photodetectors based on graphene, other two-dimensional materials and hybrid systems. *Nature nanotechnology, 9*(10), 780-793.
3. Nair, R. R., Blake, P., Grigorenko, A. N., Novoselov, K. S., Booth, T. J., Stauber, T., & Geim, A. K. (2008). Fine structure constant defines visual transparency of graphene. *science, 320*(5881), 1308-1308.
4. Vaghef-Koodehi, A., Nikoufard, M., & Rostami-Khomami, A. (2024). Voltage-tunable graphene-InP schottky photodetector with enhanced responsivity using plasmonic waveguide integration. *Physica Scripta, 99*(5), 055012.
5. Vaghef-Koodehi, A. (2025). Gate-Tunable Graphene-Enhanced Multi-Quantum Well Photodetector for Room-Temperature Mid-Infrared Detection.
6. Vaghef-Koodehi, A. (2023). "Design and simulation of graphene Schottky photodetector using InGaAsP/InP waveguide structure at 1.55 µm optical communication wavelength." Ph.D. Dissertation, Fig. 4-4, p. 89.
7. Vaghef-Koodehi, A. (2023). "Design and simulation of graphene Schottky photodetector using InGaAsP/InP waveguide structure at 1.55 µm optical communication wavelength." Ph.D. Dissertation, Fig. 3-14, p. 72.
8. Vaghef-Koodehi, A. (2023)."Design and simulation of graphene Schottky photodetector using InGaAsP/InP waveguide structure at 1.55 µm optical communication wavelength." Ph.D. Dissertation, Fig. 4-9b, p. 97.
9. Vaghef-Koodehi, A. (2023). "Design and simulation of graphene Schottky photodetector using InGaAsP/InP waveguide structure at 1.55 µm optical communication wavelength." Ph.D. Dissertation, Fig. 4-11, p. 98.
10. Freitag, M., Low, T., Xia, F., & Avouris, P. (2013). Photoconductivity of biased graphene. *Nature Photonics, 7*(1), 53-59.
11. Gan, X., Shiue, R. J., Gao, Y., Meric, I., Heinz, T. F., Shepard, K., & Englund, D. (2013). Chip-integrated ultrafast graphene photodetector with high responsivity. *Nature photonics, 7*(11), 883-887.
12. Pospischil, A., Humer, M., Furchi, M. M., Bachmann, D., Guider, R., Fromherz, T., & Mueller, T. (2013). CMOS-compatible graphene photodetector covering all optical communication bands. *Nature Photonics, 7*(11), 892-896.
13. Liu, C. H., Chang, Y. C., Norris, T. B., & Zhong, Z. (2014). Graphene photodetectors with ultra-broadband and high responsivity at room temperature. *Nature nanotechnology, 9*(4), 273-278.
14. Hu, L., Yan, J., Liao, M., Wu, L., Fang, X. (2020). "Graphene/InGaAs Schottky junction photodetector with enhanced responsivity and broadband near-infrared response." ACS

Appl. Mater. Interfaces, vol. 12, pp. 15552-15561.
15. Liu, Y., Cheng, R., Liao, L., Zhou, H., Bai, J., Liu, G., & Duan, X. (2011). Plasmon resonance enhanced multicolour photodetection by graphene. *Nature communications, 2*(1), 579.
16. Zheng, L., Zhou, X., Hu, J., Lv, L., Meng, W., Huang, Z., Zhang, W., Zhu, Y. (2019). "Graphene/Si-quantum-dot heterostructure photodetector with extended infrared response." Nanophotonics, vol. 8, pp. 1203-1211.
17. Furchi, M., Urich, A., Pospischil, A., Lilley, G., Unterrainer, K., Detz, H., ... & Mueller, T. (2012). Microcavity-integrated graphene photodetector. *Nano letters, 12*(6), 2773-2777.
18. Engel, M., Steiner, M., Lombardo, A., Ferrari, A. C., Löhneysen, H. V., Avouris, P., & Krupke, R. (2012). Light–matter interaction in a microcavity-controlled graphene transistor. *Nature communications, 3*(1), 906.
19. Echtermeyer, T. J., Britnell, L., Jasnos, P. K., Lombardo, A., Gorbachev, R. V., Grigorenko, A. N., & Novoselov, K. S. (2011). Strong plasmonic enhancement of photovoltage in graphene. *Nature communications, 2*(1), 458.
20. Fang, Z., Liu, Z., Wang, Y., Ajayan, P. M., Nordlander, P., & Halas, N. J. (2012). Graphene-antenna sandwich photodetector. *Nano letters, 12*(7), 3808-3813.
21. Schuler, S., Schall, D., Neumaier, D., Dobusch, L., Bethge, O., Schwarz, B., & Mueller, T. (2016). Controlled generation of ap–n junction in a waveguide integrated graphene photodetector. *Nano letters, 16*(11), 7107-7112.
22. Goykhman, I., Sassi, U., Desiatov, B., Mazurski, N., Milana, S., De Fazio, D., & Ferrari, A. C. (2016). On-chip integrated, silicon–graphene plasmonic Schottky photodetector with high responsivity and avalanche photogain. *Nano letters, 16*(5), 3005-3013.
23. Shiue, R. J., Gao, Y., Wang, Y., Peng, C., Robertson, A. D., Efetov, D. K., & Englund, D. (2015). High-responsivity graphene–boron nitride photodetector and autocorrelator in a silicon photonic integrated circuit. *Nano letters, 15*(11), 7288-7293.
24. Ding, Y., Cheng, Z., Zhu, X., Yvind, K., Dong, J., Galili, M., & Oxenløwe, L. K. (2020). Ultra-compact integrated graphene plasmonic photodetector with bandwidth above 110 GHz. *Nanophotonics, 9*(2), 317-325.
25. Hu, Z., Zhang, J., Hao, Z., Hao, Q., Geng, X., Zhao, Y. (2016). "Photosensitive and low dark current SWCNT/graphene/InP photodetector." Appl. Phys. Lett., vol. 108, p. 171605.
26. Saran, R., and R. J. Curry. (2014). "Ultrahigh performance fullerene free polymer solar cells using a graphene-ZnO nanorod composite layer." Sci. Rep., vol. 4, p. 5190.
27. Zhang, X., Gryczynski, I., Gryczynski, Z and Wang, H. (2008). "Metal-enhanced fluorescence emission fingerprints of five fluorophores on gold nanorods." J. Phys. Chem. B, vol. 112, pp. 14099-14102.
28. Zheng, L., Zhongzhu, L. and Guclu, S. (2020). "Wideband and high-gain graphene-based integrated THz photodetector." IEEE J. Quantum Electron., vol. 56, pp. 1-7.
29. Vakil, A., & Engheta, N. (2011). Transformation optics using graphene. *Science, 332*(6035), 1291-1294.
30. Hanson, G. W. (2008). Dyadic Green's functions and guided surface waves for a surface conductivity model of graphene. *Journal of Applied Physics, 103*(6).
31. Falkovsky, L. A. (2008). Optical properties of graphene. In Journal of Physics: conference series. IOP Publishing.
32. Novoselov, K. S., Geim, A. K., Morozov, S. V., Jiang, D. E., Zhang, Y., Dubonos, S. V., & Firsov, A. A. (2004). Electric field effect in atomically thin carbon films. *science, 306*(5696), 666-669.
33. Mak, K. F., Sfeir, M. Y., Wu, Y., Lui, C. H., Misewich, J. A., & Heinz, T. F. (2008). Measurement of the optical conductivity of graphene. *Physical review letters, 101*(19), 196405.
34. Castro Neto, A. H., Guinea, F., Peres, N. M., Novoselov, K. S., & Geim, A. K. (2009). The electronic properties of graphene. *Reviews of modern physics, 81*(1), 109-162.
35. Li, Z., Henriksen, E. A., Jiang, Z., Hao, Z., Martin, M. C., Kim, P., & Basov, D. N. (2008). Dirac charge dynamics in graphene by infrared spectroscopy. *Nature physics, 4*(7), 532-535.